Journal of Solid State Chemistry **146,** 65–72 (1999)
Article ID jssc.1999.8309, available online at http://www.idealibrary.com on IDEAL®

The Crystal Structure of $Ba_3CuRu_2O_9$ and Comparison to $Ba_3MRu_2O_9$ (M = In, Co, Ni, and Fe)

J. T. Rijssenbeek,* Q. Huang,†,‡ R. W. Erwin,† H. W. Zandbergen,§ and R. J. Cava*,[1]

*Department of Chemistry and Materials Institute, Princeton University, Princeton, New Jersey 08540; †NIST Center for Neutron Research, National Institute of Standards and Technology, Gaithersburg, Maryland 20899; ‡Department of Materials and Nuclear Engineering, University of Maryland, College Park, Maryland 20742; and §National Institute for HREM, Laboratory for Materials Science, Delft University of Technology, 2628 AL Delft, The Netherlands

Received November 4, 1998; in revised form March 12, 1999; accepted April 7, 1999

The crystal structure of $Ba_3CuRu_2O_9$, determined by powder neutron diffraction, is reported for temperatures of 18–295 K. Structural refinements by powder neutron diffraction for the previously reported compounds $Ba_3MRu_2O_9$ for M = Fe, Co, Ni, and In are also reported. All structures consist of pairs of face-shared RuO_6 octahedra interconnected by corner-sharing MO_6 octahedra. For $Ba_3CuRu_2O_9$, Jahn–Teller distortion of the CuO_6 octahedra leads to an orthorhombic symmetry structure of space group *Cmcm* with $a = 5.6723(1)$, $b = 10.1722(3)$, and $c = 14.1575(3)$ Å at 295 K. For $Ba_3FeRu_2O_9$, site occupancy disorder is found. Magnetic ordering is observed below 100, 105, and 110 K for M = Cu, Ni, and Co, respectively. The magnetic structures at low temperatures for M = Co and Ni are described and compared to previous reports. © 1999 Academic Press

INTRODUCTION

Ruthenium–based oxides have recently been of interest due to their unusual electronic and magnetic properties. Sr_2RuO_4, for example, is believed to be an exotic superconductor with $T_c = 0.93$ K (1, 2). To examine more complex ruthenium-based oxides, we have been studying compounds with the general formula $Ba_3MRu_2O_9$ where M = Fe, Co, Ni, Cu, or In, compounds in which both electronically active 3*d* and 4*d* elements may be present. We have reported their magnetic and electronic properties elsewhere (3). The compounds are all semiconducting, and, for the Cu, Ni, and Co analogs, the magnetic susceptibilities indicate the presence of a magnetic transition at approximately 100 K. The compounds with M = In and Ni were originally prepared by Schaller and Kemmler-Sack (4) and Donohue *et al.* (5), and the Co and Fe compounds were originally prepared by Treiber *et al.* (6). Powder neutron diffraction studies of the crystal structures and magnetic ordering for $Ba_3MRu_2O_9$ with M = Zn, Ni, and Co have been reported by Lightfoot and Battle (7). These compounds have the hexagonal barium titanate structure type with Ru_2O_9 dimers, made from face shared RuO_6 octahedra, interconnected by corner-sharing MO_6 octahedra. In the course of our investigation, we discovered the existence of a Cu analog, $Ba_3CuRu_2O_9$, with a significantly distorted structure. Here we present the results of neutron diffraction powder profile refinement of the ambient and low temperature crystal structures for that compound. The results show that the distortion is due to the presence of a Jahn–Teller distortion of the CuO_6 octahedron, indicating formal presence of Cu^{2+} and Ru^{5+} in the same compound. For comparison purposes, refinements of the structures of the related compounds $Ba_3MRu_2O_9$ for M = In, Fe, Co, and Ni are also presented. For the two latter phases, the magnetic scattering was sufficiently strong that the magnetic structures could be determined at low temperatures. Where directly comparable, our results on those compounds are in agreement with previous results (e.g., Ref. 7), except for the Co analog at low temperatures, where we do not find a distortion from the ideal hexagonal structure.

EXPERIMENTAL

Barium carbonate, RuO_2, and the appropriate metal oxide (Fe_2O_3, Co_3O_4, NiO, CuO, or In_2O_3) were mixed in stoichiometric amounts and ground in an agate mortar. The mixtures were heated in aluminum oxide crucibles in air from 800 to 1100°C in 150°C increments with grinding after each 48-h step, with reheating at 1100°C until the materials were single phase.

X-ray powder diffraction patterns, which were employed to determine phase purity, were obtained on a Rigaku Miniflex diffractometer using Cu$K\alpha$ radiation. Electron diffraction studies were performed on a Phillips CM300 electron microscope to determine the crystallographic unit cell

[1]To whom all corrspondence should be addressed.

0022-4596/99 $30.00

for $Ba_3CuRu_2O_9$. The powder neutron diffraction patterns were obtained at the reactor of the National Institute of Standards and Technology Center for Neutron Research using the BT-1 high-resolution powder diffractometer with neutron beams of wavelength 1.5401(1) Å. Collimators with horizontal divergences of 15′, 20′, and 7′ of arc full width at half maximum were used before and after the monochromator and after the sample, respectively. The intensities were measured in steps of 0.05° in the 2θ range 3°–168°. Data were collected at 295 K to elucidate the crystal structures. The structural parameters were determined by using the program GSAS (8). Data were collected at low temperatures to allow the determination of the magnetic structures. The magnetic order parameters for M = Cu, Ni, Co, and Fe were measured using the BT-9 triple-axis spectrometer with a pyrolytic graphite PG(002) monochromator, which produces much stronger neutron intensity. The neutron scattering amplitudes for Ba, Ru, In, Fe, Co, Ni, Cu, and O are 0.525, 0.721, 0.406, 0.954, 0.253, 1.03, 0.772, and 0.581×10^{-12} cm, respectively.

RESULTS

$Ba_3CuRu_2O_9$

The X-ray powder diffraction pattern for $Ba_3CuRu_2O_9$ was similar to that for the other materials in this chemical family, indicating that the phase was related to them, but the pattern of splitting of the peaks showed that the symmetry of the phase was clearly lower. The crystallographic unit cell was determined to be of orthorhombic symmetry by analysis of the reciprocal lattice in a small single crystal by electron diffraction, with approximate cell dimensions $a = 5.67$, $b = 10.17$, and $c = 14.16$ Å. This orthorhombic supercell is related to the ideal hexagonal subcell of this structure type by $(a, b, c)_{\text{ortho}} = (1, 0, 0/-1, 2, 0/0, 0, 1)(a, b, c)_{\text{hex}}$. The orthorhombic cell parameters determined in the electron diffraction experiments were then employed to index and refine the powder X-ray diffraction data, verifying the correctness of the cell.

The orthorhombic cell of $Ba_3CuRu_2O_9$ at ambient temperature is a more highly distorted version of the cell reported for the structure of $Ba_3CoRu_2O_9$ (7) at 2 K, in space group *Cmcm*. For a dimensionally undistorted orthorhombic cell derived from the hexagonal cell, the orthorhombic cell parameters a and b are related by $a/b = 1/\sqrt{3}$ (0.577). For the reported case of $Ba_3CoRu_2O_9$ at 2 K, $a/b = 5.745/9.9177 = 0.579$, and in the present case, for $Ba_3CuRu_2O_9$, $a/b = 5.672/10.172 = 0.557$, more distorted from the ideal. The a/b ratio for $Ba_3CuRu_2O_9$ is independent of temperature within experimental uncertainty, being 0.557, 0.558, and 0.558 at 295, 150, and 18 K, respectively. There is therefore no indication that a transition to a hexagonal symmetry state at higher temperature is being initiated in this temperature range. The crystal structure refined very well using as an initial model the reported 2 K structure of $Ba_3BoRu_2O_9$. No further structural distortion was found at low temperatures. The final positional coordinates and agreement factors are shown in Table 1 for all temperatures. The observed and calculated neutron diffraction profile at 18 K is shown in Fig. 1. Important interatomic distances and angles for the three temperatures studied are presented in Table 2.

The crystal structure of $Ba_3CuRu_2O_9$ is shown in Fig. 2. The structure is seen in its basic nature to be that of six-layer $BaTiO_3$. The structural feature of primary interest is the mixing of perovskite-like metal-oxygen octahedron linking and face sharing octahedron linking, an arrangement which might be expected to be energetically unfavorable due to metal–metal repulsion. The coordination polyhedra are presented in Fig. 3. Figure 3a shows the Ru–Ru octahedra sharing a face in a dimer-like arrangement, with a Ru–Ru separation of across the shared face of $\sim$2.7 Å. This dimer is corner-shared with the CuO_6 octahedra, in a perovskite

TABLE 1
Structural Parameters for $Ba_3CuRu_2O_9$ and Selected Interatomic Distances (Å) and Angles (°)

Atom	Parameter	295 K	150 K	18 K
	a (Å)	5.6723(1)	5.6637(1)	5.6623(1)
	b (Å)	10.1722(3)	10.1511(2)	10.1434(3)
	c (Å)	14.1575(3)	14.1372(2)	14.1357(3)
	V (Å^3)	816.88(4)	812.79(3)	811.88(4)
Ba(1)	y	−0.0141(5)	−0.0136(5)	−0.0157(6)
	B (Å^2)	0.74(4)	0.49(3)	0.32(4)
Ba(2)	y	0.3245(4)	0.3244(4)	0.3237(4)
	z	0.0903(2)	0.0900(2)	0.0911(2)
	B (Å^2)	0.74(4)	0.49(3)	0.32(4)
Ru	y	0.3489(3)	0.3488(2)	0.3489(3)
	z	0.8454(2)	0.8449(1)	0.8454(2)
	B (Å^2)	0.68(3)	0.52(3)	0.33(3)
Cu	B (Å^2)	0.68(3)	0.52(2)	0.33(3)
O(1)	y	0.5013(5)	0.5009(5)	0.5016(5)
	B (Å^2)	0.58(7)	0.44(6)	0.35(8)
O(2)	x	0.2695(6)	0.2713(5)	0.2710(6)
	y	0.2253(3)	0.2258(3)	0.2262(3)
	B (Å^2)	0.63(5)	0.42(5)	0.10(5)
O(3)	y	0.8087(4)	0.8094(3)	0.8099(4)
	z	0.0844(3)	0.0839(2)	0.0833(3)
	B (Å^2)	0.95(6)	0.81(6)	0.50(6)
O(4)	x	0.2511(6)	0.2513(5)	0.2517(6)
	y	0.0743(3)	0.0724(2)	0.7176(3)
	z	0.0842(2)	0.0842(2)	0.0846(2)
	B (Å^2)	1.11(4)	0.74(3)	0.76(4)
	R_p (%)	5.00	4.86	5.61
	R_{wp} (%)	6.31	6.18	7.04
	χ^2	1.813	1.733	2.343

Note. Space group *Cmcm*; $z = 4$. The atomic positions: Ba(1): $4c(0, y, 1/4)$; Ba(2): $8f(0, y, z)$; Ru: $8f(0, y, z)$; Cu: $4a(0, 0, 0)$; O(1): $4c(0, y, 1/4)$; O(2): $8g(x, y, 1/4)$; O(3): $8f(0, y, z)$; O(4): $16h(x, y, z)$. Constrained: $B_{\text{Ba}(1)} = B_{\text{Ba}(2)}$, $B_{\text{Ru}} = B_{\text{Cu}}$.

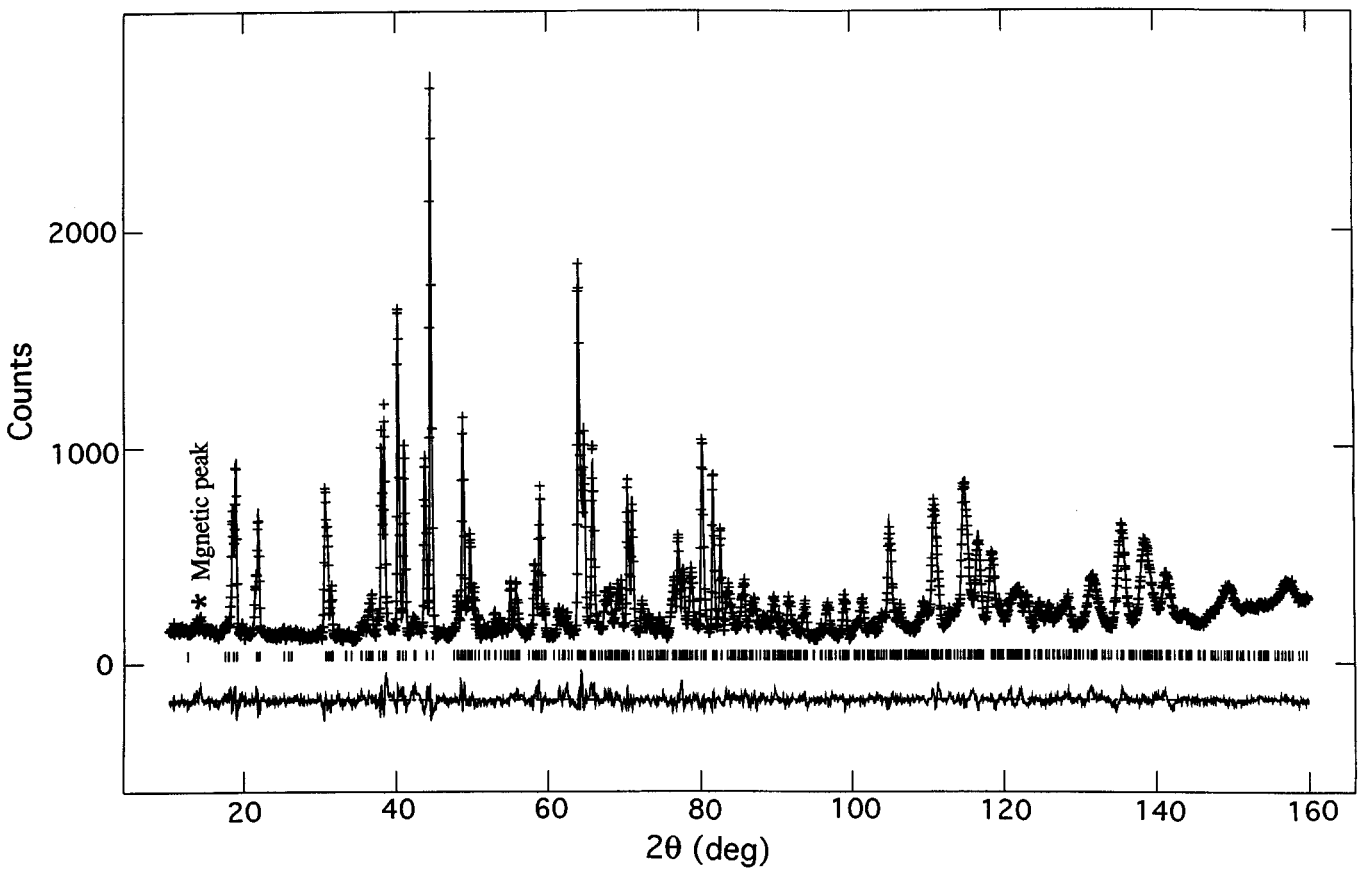

FIG. 1. Plot of the observed and calculated neutron diffraction intensity profile for $Ba_3CuRu_2O_9$ at 18 K. The lower part shows the difference plot, I(obs) − I(calc), and the vertical lines indicate the angular positions of the Bragg reflections.

arrangement, with Ru–O–Cu bond angles near 180°. The CuO_6 octahedra (Fig. 3a) are highly distorted, with four in-plane short bonds (2.00 Å) and two out-of-plane long bonds (2.28 Å), similar to those found in La_2CuO_4 (9). This suggests that the Cu electronic configuration is $3d^9$, or Cu^{2+}. These octahedra occur in triangular planes perpendicular to the *c*-axis with the Cu atoms separated by the *a*-axis length (∼5.7 Å), resulting in no direct Cu–Cu or Cu–O–Cu exchange pathways. The same is true for the analogs with the other 3*d* *M* elements, where the only significant structural difference is the regularity of the *M*–O octahedra.

The RuO_6 octahedra are also distorted, but not to the same degree or in the same manner. There are three shorter Ru–O distances (1.89 Å) and three longer Ru–O distances (2.03 Å). The longer Ru–O distances are to the Ru in the shared face between octahedra, due to the repulsion of the Ru. For a charge distribution of Ba^{2+}, Cu^{2+}, and O^{2-}, the formal charge for Ru in this compound is 5+. The average Ru–O distance observed here, 1.96 Å, is consistent with what has been observed in other compounds (10). The BaO_{12} polyhedra (Fig. 3b) are cuboctahedra (Ba(2)–O) and anticuboctahedra (Ba(1)–O). These coordination environments are typical of that of Ba in close-packed oxygen arrays, where, due to its comparable size, Ba substitutes for one of the O in either a CCP oxygen lattice (cuboctahedron) or an HCP oxygen lattice (anticuboctahedron).

Comparison to $Ba_3MRu_2O_9$

The initial model for the structures for *M* = Fe, Co, Ni, and In was taken as that reported by Treiber *et al.* (6) for ambient temperature $Ba_3CoRu_2O_9$. The structures were all refined in space group $P6_3/mmc$ with final weighed profile *R* factors (R_{wp}) between 5 and 6% both at ambient temperature and at temperatures near 10 K. The final positional parameters and agreement factors are presented in Table 3. Important interatomic spacings and bond angles are presented in Table 4.

For all compounds, the two octahedrally coordinated metal atoms (Ru and *M*) were allowed to vary their proportions on the two possible metal sites. The neutron scattering lengths are sufficiently different for the diffracted intensities to be sensitive to the distribution. These refinements found

TABLE 2
Selected Interatomic Distances (Å) and Angles (°) for $Ba_3CuRu_2O_9$

		295 K	150 K	18 K
Ba(1)–O(1)	×2	2.8405(5)	2.8357(4)	2.8365(5)
–O(2)	×2	2.876(5)	2.875(6)	2.893(6)
–O(2)	×2	2.955(6)	2.945(6)	2.922(6)
–O(3)	×2	2.958(5)	2.957(5)	2.947(5)
–O(4)	×4	2.883(3)	2.878(3)	2.879(3)
Ba(2)–O(1)		2.889(5)	2.885(5)	2.881(5)
–O(2)	×2	2.910(3)	2.911(3)	2.895(3)
–O(3)		2.819(5)	2.809(5)	2.813(5)
–O(3)	×2	2.8419(4)	2.8373(3)	2.8368(4)
–O(4)	×2	2.934(5)	2.928(4)	2.927(5)
–O(4)	×2	2.892(5)	2.887(4)	2.884(5)
–O(4)	×2	3.032(3)	3.025(3)	3.044(3)
Ru(1)–O(1)		2.036(5)	2.032(4)	2.030(5)
–O(2)	×2	2.026(3)	2.013(3)	2.020(3)
–O(3)		1.886(5)	1.895(4)	1.900(5)
–O(4)	×2	1.905(4)	1.904(3)	1.899(4)
Ru–O(average)		**1.964**	**1.960**	**1.961**
Cu(3)–O(1)	×2	2.283(4)	2.270(4)	2.259(4)
–O(4)	×4	1.998(3)	1.996(3)	1.997(3)
Ru–Ru		2.701(4)	2.684(4)	2.698(5)
O(1)–Ru–O(2)		80.6(1)	80.9(1)	80.7(1)
O(1)–Ru–O(3)		170.3(2)	170.8(2)	170.4(2)
O(1)–Ru–O(4)		91.9(1)	91.8(1)	97.7(1)
O(2)–Ru–O(2)		80.4(2)	80.1(2)	79.9(2)
O(2)–Ru–O(3)		92.0(2)	92.0(1)	92.0(2)
O(2)–Ru–O(4)		169.8(1)	169.9(1)	169.5(2)
O(2)–Ru–O(4)		91.7(1)	91.87(9)	91.9(1)
O(3)–Ru–O(4)		94.7(1)	94.4 (1)	94.8(1)
O(4)–Ru–O(4)		95.7(2)	95.4(2)	95.6(2)
O(3)–Cu–O(3)		180	180	180
O(3)–Cu–O(4)		90.1(1)	90.13(9)	90.0(1)
O(3)–Cu–O(4)		89.9(1)	89.87(9)	90.0(1)
O(4)–Cu–O(4)		180	180	180
O(4)–Cu–O(4)		89.1(2)	89.1(1)	89.9(2)
O(4)–Cu–O(4)		90.9(2)	91.0(1)	91.0(2)

the M atoms to be ordered in the 2a site for M = Co, Ni, and In, indicating that the structure contains dimers of Ru–Ru octahedra sharing faces, joined to neighboring dimers by MO_6 octahedra sharing corners with the dimer in fully ordered structures. In the case of M = Fe, however, a considerable amount of mixing between Fe and Ru was found, although Fe prefers the 2a site. Of the one Fe per formula unit, 0.6 are found in the isolated octahedron (2a site) and 0.4 are found mixed in with the Ru in the dimer site (4f site), in a highly disordered structure. This mixing of the Ru and Fe ions on the available sites, as well as the electronic structure of Fe, makes the magnetic properties of the Fe analog considerably different from the other materials (3).

The MO_6 octahedra are constrained by the structural symmetry to have six equal M–O bondlengths and are highly regular in shape, as can be seen in the entries in Table 4. For the RuO_6 octahedra, however, comparison of the bond lengths and angles for the different structures reveals an interesting systematic behavior. The shapes of the octahedra depend on whether the 3d ion is in a divalent or a trivalent state, resulting in a formal Ru valence of 5+ or 4.5+, respectively. For In and Fe, which are trivalent (3), the $Ru^{4.5+}$–O octahedra are regular, with a difference in Ru–O bondlengths of only 0.01 Å. In addition, the Ru–Ru separation across the shared face (2.51 Å for M = In and 2.60 Å for M = Fe, respectively) is the shortest, indicating that for the lower charged Ru there is less distortion due to Ru–Ru repulsion (for the Fe compound there is also some Fe in these sites). For the more highly charged Ru, found for M = Cu, Co, and Ni, all of which are divalent (3, 7), the bond lengths are distorted to accommodate increased Ru–Ru repulsion, with increase in Ru–O bond lengths of 0.14, 0.12, and 0.11 Å to the oxygens in the shared faces compared to those at the top and bottom of the dimer, and also increased Ru–Ru distances, of 2.7 Å.

For $Ba_3MRu_2O_9$ for M = Cu, Ni, and Co, a magnetic transition has been observed near 100 K in magnetic susceptibility measurements (3). Refinements of the magnetic structures at low temperatures for M = Ni and Co have been reported by Lightfoot *et al.* (7). The present results confirm the results of that study. For $Ba_3CoRu_2O_9$, we observed antiferromagnetic diffraction peaks in the low angle region at 15 K. These are indexed by an orthorhombic superlattice related to the hexagonal structural unit cell by $(a,b,c)_{ortho} = (1,0,0/-1,2,0/0,0,1)\ (a,b,c)_{hex}$, as shown in Fig. 3b. The magnetic structure model determined in Ref. (7), when used in the refinement for the magnetic structure, gave very good agreement of the observed and calculated magnetic intensities. The magnetic moments determined at 15 K are 2.84(8) μ_B and 1.16(9) μ_B for Co and Ru, respectively, comparable with those found earlier, 2.71 and 1.44 μ_B. The magnetic moments for both Co and Ru lie on the a–b plane and are ordered ferromagnetically along the a (or b) direction and antiferromagnetically along the b (or a) and c direction (see Fig. 3b).

For $Ba_3NiRu_2O_9$, we observed only one distinct peak of magnetic origin at 8 K. This peak had an index of (111), which is a systematic absence in the space group $P6_3/mmc$. Some extra intensity of magnetic origin was found to be overlapping with the (102), (103), and (104) nuclear Bragg peaks. This pattern of magnetic scattering suggests that (i) the magnetic structure has the same unit cell as the crystallographic unit cell and therefore the magnetic moments order ferromagnetically in the a–b plane, and (ii) antiferromagnetic ordering may occur along the c-axis. These

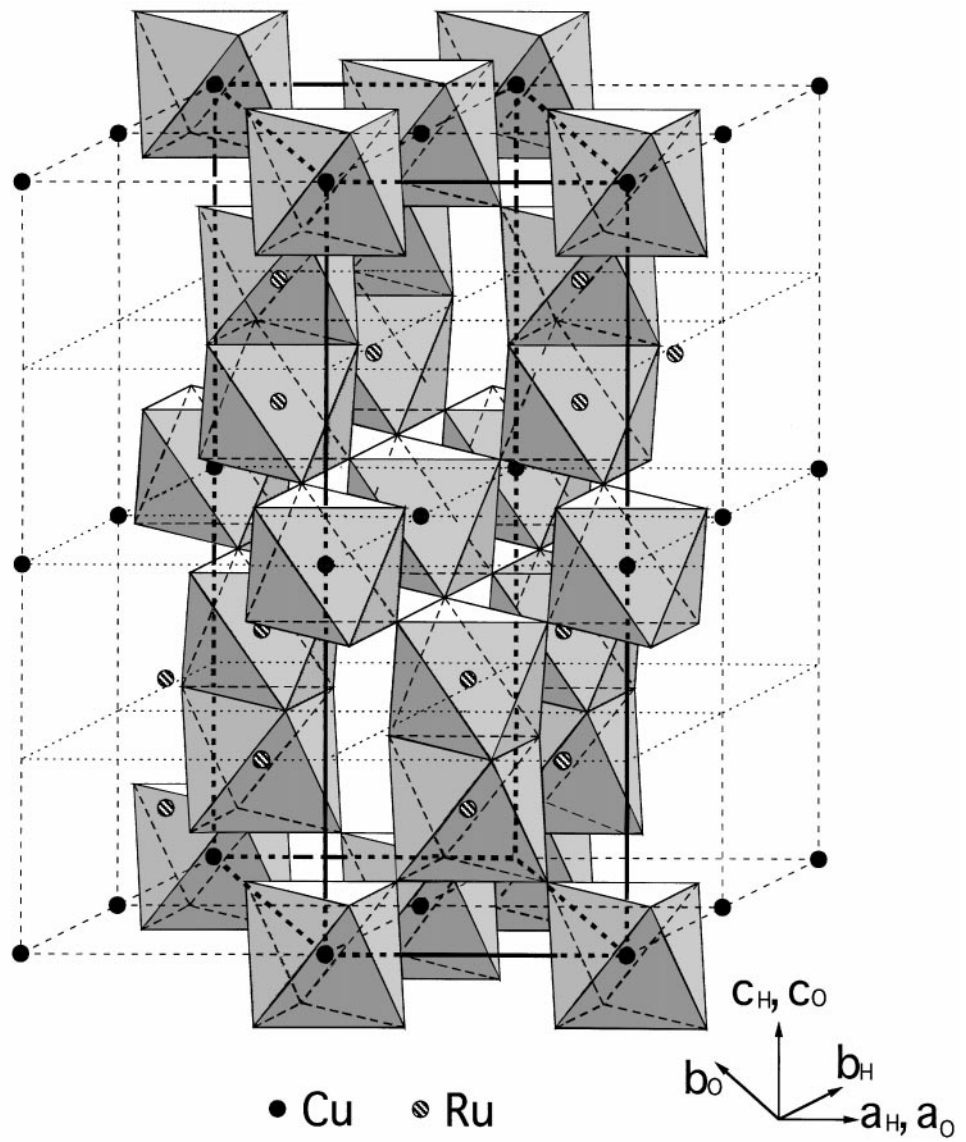

FIG. 2. Schematic representation of the Ru and Cu octahedra packing in the supercell for $Ba_3CuRu_2O_9$ and the relationship between the orthorhombic supercell (thick line) and the hexagonal subcell (thin line).

considerations are consistent with the magnetic model for this compound reported in Ref. (7). When that model is used in further refinement of our data, the agreement factors (compared to nuclear scattering only) R_p, R_{wp}, and χ^2 improve from 4.05, 5.20, and 1.341 to 3.97, 5.10, and 1.291, respectively. Figure 3c shows a schematic representation of the magnetic structure. In this case, the spin direction is parallel to the *c*-axis, with ferromagnetic ordering in the *a*–*b* plane and antiferromagnetic ordering between layers along the *c*-axis. Magnetic moments of 1.8(1) and 1.0(1) μ_B were obtained in the final refinement for Ni and Ru, respectively, compared to 1.7 and 1.5 μ_B found in Ref. (7). We do not know why the magnetic ordering schemes for the Co and Ni compounds are different.

We observed only two weak magnetic reflections, at $2\Theta = 13.65^\circ$ and 14.25°, in $Ba_3CuRu_2O_9$. The intensity information was not sufficient to elucidate the magnetic structure. Figure 4 shows the temperature dependence of the intensities of the reflection at $2\Theta = 14.25^\circ$ and the $(\frac{1}{2}01)$, (103), and (101) reflections (referred to the nuclear unit cell) for Cu and M = Co, Ni, and Fe, respectively. The magnetic transition temperatures are found to be only a few degrees different for the Cu, Co, and Ni compounds, consistent with the observed magnetic susceptibilities (3) (Fig. 5). For the Fe compound, however, the behavior of the (101) peak intensity, linearly decreasing as the temperature increases, is much more like the effect of the Debye temperature (i.e., the behavior of a thermal vibration parameter) of the crystal

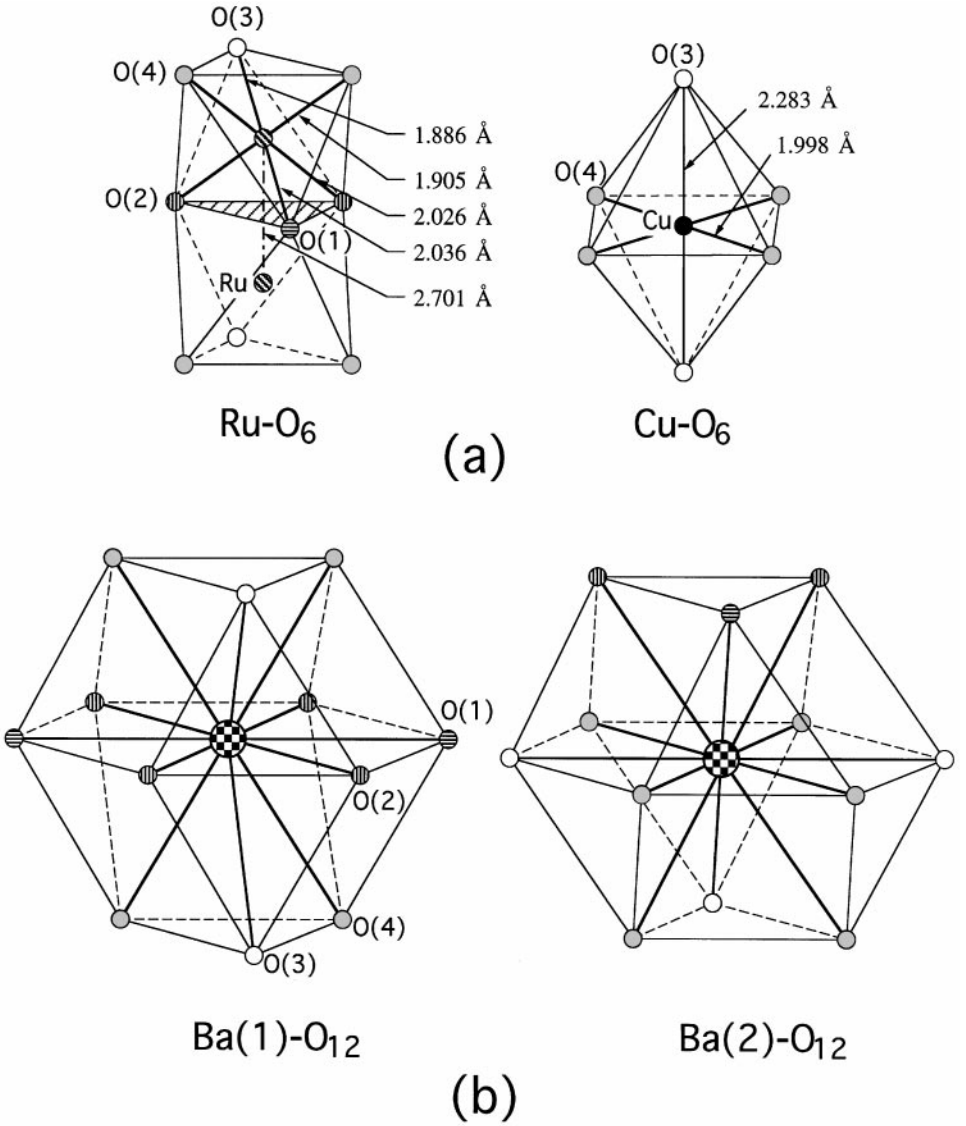

FIG. 3. The coordination polyhedra in $Ba_3CuRu_2O_9$. (a) the RuO_6 octahedra sharing a face and the CuO_6 octahedron, and (b) the BaO_{12} polyhedra.

than that of magnetic ordering. This again is consistent with the magnetic data (3), where no magnetic ordering was observed for the Fe-based analog in this temperature regime.

CONCLUSION

The neutron diffraction data have shown that in the members of this family studied, there is a strong tendency toward ordering of the 3*d* atoms in the isolated MO_6 octahedra, maintaining an ordered array of Ru–Ru dimers, except for the case of iron, where the ordering breaks down. In the case of M = Mn (12), a disordered structure has also been reported, consistent with the trend observed here. Although $BaRuO_3$ itself is a metallic conductor (13), all of the members of the $Ba_3MRu_2O_9$ family are nonmetallic. This result is not surprising for M = In because the indium–oxygen orbital overlap is expected to be poor. For the transition metals, however, this finding was unexpected, as it indicates nonmetallic behavior over a wide range of electron counts. At room temperature the Ru–Ru distances ($\sim$2.6 Å) are short enough to allow good orbital overlap and sharing of electrons. The 180° Ru–O–M bonds are expected to have the correct geometry to allow conduction through the octahedral site thus coupling the ruthenium dimers. This, however, does not occur. The temperature dependence of the resistivities suggests that the M atoms in the octahedral sites effetively lead to localization of the charge carriers and isolation of the Ru dimers, implying that the energies of the

TABLE 3
Structural Parameters for $Ba_3MRu_2O_9$ (M = In, Co, Ni, and Fe)

		(M=)	In	Co		Ni		Fe^{11}	
Atom	Parameter	295 K	8.6 K	295 K	15 K	295 K	8.6 K	295 K	15 K
	a (Å)	5.8181(3)	5.8033(3)	5.7517(1)	5.7370(1)	5.74233(9)	5.7275(8)	5.7248(2)	5.7120(2)
	b (Å)	14.306(1)	14.288(1)	14.1229(4)	14.0932(5)	14.1040(3)	14.0729(3)	14.0652(7)	14.0347(8)
	V (Å^3)	419.38(6)	416.73(5)	404.61(2)	401.71(2)	402.76(2)	399.80(2)	399.21(4)	396.57(4)
Ba(1)	B (Å^2)	0.91(5)	0.40(5)	0.61(3)	0.25(3)	0.54(2)	0.23 (2)	0.45(5)	0.10(4)
Ba(2)	z	0.0900(4)	0.0877(4)	0.0898(2)	0.0897(2)	0.0898(2)	0.0886(2)	0.0908(3)	0.0901(3)
	B (Å^2)	0.91(5)	0.40(5)	0.61(3)	0.25(3)	0.54(2)	0.23(2)	0.45(5)	0.10(4)
Ru/M	z	0.8380(3)	0.8376(2)	0.8450(2)	0.8449(2)	0.8452(1)	0.8448(1)	0.8435(3)	0.8430(3)
	B (Å^2)	0.48(4)	0.21(4)	0.45(3)	0.25(3)	0.55(1)	0.33(1)	0.80(4)	0.59(4)
	n	1/0	1/0	1/0	1/0	1/0	1/0	0.81(4)/0.19(4)	0.80(2)/0.20(2)
M/Ru	B(Å^2)	0.48(4)	0.21(4)	0.45(3)	0.25(3)	0.55(1)	0.33(1)	0.80(4)	0.59(4)
	n	1/0	1/0	1/0	1/0	1/0	1/0	0.59(5)/0.41(5)	0.60(5)/0.40(5)
O(1)	x	0.5137(4)	0.5123(4)	0.5142(3)	0.5132(3)	0.5145(2)	0.5141(2)	0.5131(4)	0.5133(4)
	B (Å^2)	0.70(6)	0.47(5)	0.60(3)	0.41(4)	0.59(3)	0.30(2)	0.56(6)	0.34(6)
O(2)	x	0.8298(4)	0.8295(4)	0.8299(3)	0.8307(3)	0.8300(2)	0.8298(2)	0.8334(4)	0.8336(4)
	z	0.0856(2)	0.0855(2)	0.0836(1)	0.0836(1)	0.08308(8)	0.08307(8)	0.0811(2)	0.0812(2)
	B (Å^2)	1.25(5)	0.77(4)	0.87(2)	0.47(2)	0.77(2)	0.42(2)	0.95(5)	0.50(4)
	R_p (%)	4.91	5.26	4.20	4.62	4.05	4.03	4.60	4.94
	R_{wp}(%)	6.21	6.64	5.19	5.88	5.07	5.21	5.60	6.12
	χ^2	1.178	1.238	0.871	1.128	1.260	1.345	1.251	1.483

Note. Space group $P6_3/mmc$, $z = 2$. The atomic positions: Ba(1): $2b(0, 0, 1/4)$; Ba(2): $4f(1/3, 2/3, z)$; Ru: $4f(1/3, 2/3, z)$; M: $2a(0, 0, 0)$; O(1): $6h(x, 2x, 1/4)$; O(2): $12k(x, 2x, z)$. Constrained: $B_{Ba(1)} = B_{Ba(2)}$, $B_{Ru} = B_M$.

3d transition metal states are quite different from those of the Ru. The presence of the Jahn–Teller distortion in the Cu compound, in conjunction with the insulating behavior, suggests that electron–lattice interactions may be strong in this structure type and that the carriers may be trapped in bound polarons.

TABLE 4
Selected Interatomic Distances (Å) and Angles (°) for $Ba_3MRu_2O_9$ (M = In, Co, Ni, and Fe)

		(M=)	In	Co		Ni		Fe	
		295 K	8.6 K	295 K	15 K	295 K	8.6 K	295 K	15 K
Ba(1)–O(1)	×6	2.9123(3)	2.9043(2)	2.8793(1)	2.8715(2)	2.8748(1)	2.8672(1)	2.8658(3)	2.8593(2)
Ba(1)–O(2)	×6	2.911(4)	2.909(3)	2.897(2)	2.886(2)	2.899(2)	2.893(2)	2.906(4)	2.896(3)
Ba(2)–O(1)	×3	2.923(6)	2.935(6)	2.892(3)	2.880(4)	2.890(2)	2.894(2)	2.860(5)	2.859(5)
Ba(2)–O(2)	×6	2.9099(3)	2.9020(2)	2.8774(2)	2.8700(2)	2.8729(1)	2.86502 (9)	2.8666(3)	2.8597(3)
Ba(2)–O(2)	×3	3.002(5)	2.967(5)	2.940(3)	2.937(3)	2.930(2)	2.907(2)	2.923(5)	2.914(5)
Ru–O(1)	×3	1.990(4)	1.993(4)	2.027(3)	2.028(3)	2.023(2)	2.018(2)	2.000(5)	1.993(5)
Ru–O(2)	×3	1.975(4)	1.971(4)	1.913(3)	1.916(3)	1.913(1)	1.910(2)	1.968(5)	1.967(5)
Ru–O (average)		**1.9825**	**1.982**	**1.970**	**1.972**	**1.968**	**1.964**	**1.984**	**1.980**
O(1)–Ru–O(1)		84.3(2)	84.8(2)	81.0(1)	81.3(1)	80.74(8)	81.02(7)	82.1(2)	82.3(2)
O(1)–Ru–O(2)		91.60(8)	91.53(7)	91.74(5)	91.54(5)	91.91(4)	91.92(4)	92.36(8)	92.29(8)
O(2)–Ru–O(2)		91.3(2)	92.0(2)	94.8(1)	94.9(1)	94.65(8)	94.40(7)	92.7(2)	92.7(2)
O(1)–Ru–O(2)		174.4(2)	175.0(2)	174.3(1)	174.5(1)	170.3(1)	170.68(9)	172.6(2)	172.8(2)
Ru–O(1)–Ru		78.5(2)	77.8(2)	82.9(1)	82.5(1)	83.2(1)	82.81(9)	81.4(3)	81.1(3)
M–O(2)	×6	2.107(4)	2.104(3)	2.065(2)	2.054(2)	2.057(2)	2.054(1)	2.009(4)	2.005(4)
O(2)–M–O(2)		89.6(1)	89.7(1)	90.56(8)	90.36(9)	90.77(6)	90.80(6)	91.4(1)	91.3(1)
O(2)–M–O(2)		90.4(1)	90.3(1)	89.44(8)	89.64(9)	89.23(6)	89.20(6)	88.6(1)	88.7(1)
O(2)–M–O(2)		180	180	180	180	180	180	180	180
Ru–O(2)–M		178.1(2)	178.4(2)	176.9(1)	176.7(1)	177.18(9)	177.39(8)	179.0(2)	180.0(2)
Ru–Ru		2.517(7)	2.503(7)	2.684(4)	2.674(5)	2.686(4)	2.669(3)	2.607(9)	2.591(9)

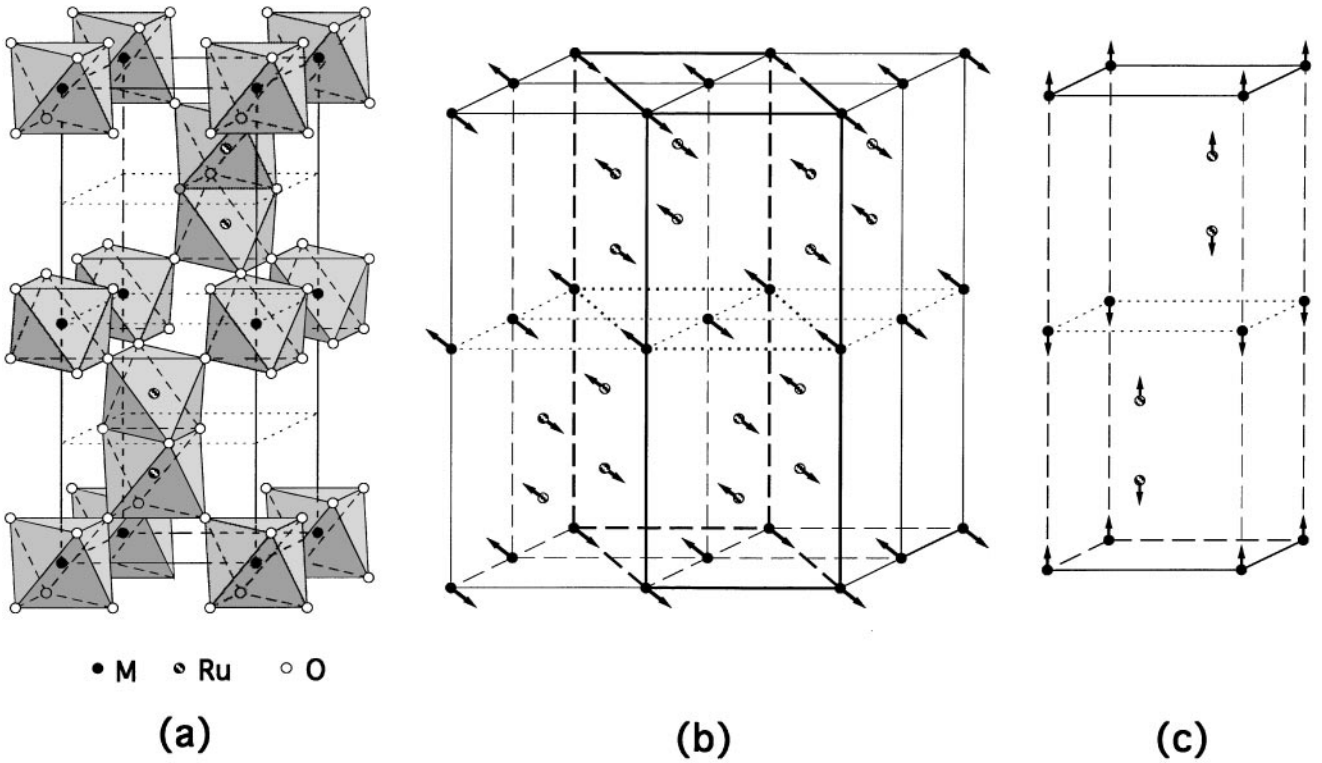

FIG. 4. Schematic representation of (a) the Ru and M ocrtahedra packing in the six-layer structure common to members of the $Ba_3MRu_2O_9$ series of compounds, with M = Fe, Co, Ni, and In. (b) The magnetic structure for $Ba_3CoRu_2O_9$, and (c) the magnetic structure for $Ba_3NiRu_2O_9$. In the $Ba_3FeRu_2O_9$ case the Ru and Fe are partially mixed in the different types of octahedra.

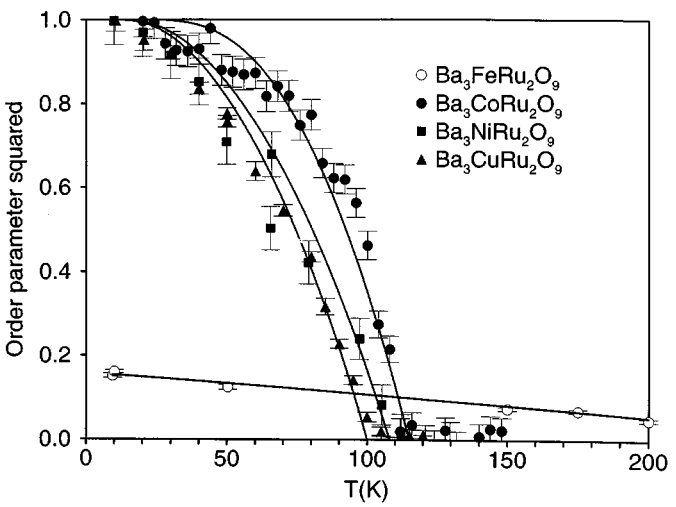

FIG. 5. Temperature dependence of the normalized intensities (which are proportional to the square of the magnetic order parameter) for $Ba_3MRu_2O_9$ for M = Co, Ni, and Cu. The diffraction peaks were measured at $Q = 0.772$ Å^{-1} $(1/201)_{hex}$, 1.8408 Å^{-1} $(103)_{hex}$, and 1.01 Å^{-1}, respectively. The fractional change in intensity, compared to room temperature, is also plotted for M = Fe, measured at $Q = 1.347$ Å^{-1} $(101)_{hex}$. Lines drawn are guides to the eye.

REFERENCES

1. Y. Maeno, H. Hashimoto, K. Yoshida, S. Nishizaki, T. Fujita, J. G. Bednorz, and F. Lichtenberg, *Nature* **372,** 532 (1994).
2. Y. Maeno, *Physica C* **282–287,** 206 (1997).
3. J. T. Rijssenbeek, P. Matl, B. Batlogg, N. P. Ong, and R. J. Cava, *Phys. Rev. B* **58,** 10,315 (1998).
4. H.-U. Schaller and S. Kemmler-Sack, *Z. Anorg. Allg. Chem.* **473,** 178 (1981).
5. P. C. Donohue, L. Katz, and R. Ward, *Inorg. Chem.* **5,** 3, 339 (1966).
6. U. Treiber, S. Kemmler-Sack, and U. Ehmann, *Z. Anorg. Allg. Chem.* **487,** 189 (1982).
7. P. Lightfoot and P. D. Battle, *J. Solid State Chem.* **89,** 174 (1990).
8. A. C. Larson and R. B. Von Dreele, "General Structure Analysis System," Report LAUR086-748, Los Alamos National Laboratory, Los Alamos, NM, 1990.
9. V. B. Grande, Hk. Muller-Buschabaum, and M. Schweizer, *Z. Anorg. Allg. Chem.* **428,** 120 (1977).
10. R. D. Shannon, *Acta Cryst. A* **32,** 751 (1976).
11. For the M = Fe sample employed in the neutron diffraction study, three phases coexist: 8.29% $Ba_3FeRu_2O_9$, 5.0% 9-layer $BaRuO_3$, and 5.8% 4-layer $BaRuO_3$. The refined structure of $Ba_3FeRu_2O_9$ is not affected.
12. S. Frenzen and H. K. Muller-Buschbaum, *Z. Naturforsch.* **50b,** 585 (1995).
13. M. Shepard, S. McCall, G. Cao, and J. E. Crow, *J. Appl. Phys.* **81,** 4978 (1997).